A 3D elasto-plastic soil model for lateral buckling analysis

Hededal, Ole; Strandgaard, Torsten

Published in:
Proceedings of the Eighteenth (2008) International Offshore and Polar Engineering Conference

Publication date:
2008

Document Version
Publisher's PDF, also known as Version of record

Proceedings of the Eighteenth (2008) International Offshore and Polar Engineering Conference
Vancouver, BC, Canada, July 6-11, 2008

ISBN 978-1-880653-70-8 (Set); ISBN 1-880653-68-0 (Set)

A 3D elasto-plastic soil model for lateral buckling analysis

Ole Hededal
Technical University of Denmark
Lyngby, Denmark

Torsten Strandgaard
GeoLine APS
Bagsværd, Denmark

ABSTRACT
Modeling the lay-down of pipelines and subsequently the in-service conditions for a pipeline involves definition of a pipe-soil interaction model. A generalized true 3D elasto-plastic spring element based on an anisotropic hardening/degradation model for sliding is presented. The basis for the model is the elasto-plastic framework. A generic format is selected, allowing different yield criteria and flow rules to be implemented in a simple way. The model complies to a finite element format allowing it to be directly implemented into a standard finite element code. Examples demonstrating the robustness of the model are presented.

INTRODUCTION
Modeling the installation and subsequent service condition of a pipeline is a complex task. The models for global analysis of a pipeline are most often based a Winkler approach. The models must thus comprise a robust beam description allowing for large displacements and a strategy for contact with the seabed. Once in contact, the interaction between the pipeline and the seabed must be described in a simple, yet realistic way. During pipelay the model should be able to describe touchdown with over-penetration and possible vertical suction breakout if the contact point is lifted later on as well as horizontal movements of the pipeline. In the operation phase when the pipeline is unburied or partially buried, the lateral soil resistance plays a significant role in on-bottom stability and lateral buckling. This paper concentrates on the modeling of unburied and partially buried pipelines and apply mainly to deepwater pipelines, where the loads governing the design are those related to walking (ratcheting) and lateral buckling, White and Randolph (2007).
Browsing the literature on this topic reveals a significant emphasis on experimental investigations of the problem using e.g. physical modeling in centrifuges or large-scale testing, Lambrakos (1985), Bruton et al. (2006), Bruton et al. (2007) and Cheuk et al. (2007). The experimental work gives valuable information on principal behavior and is vital for the calibration of models. Several parametric models have been developed accounting for vertical and horizontal resistance, Cathie et al. (2005) and White and Randolph (2007). However, the implementation of these observations into design models based on numerical methods appears to be restricted to Winkler models formulated in terms of systems of 3 uncoupled springs i.e. in vertical, lateral and axial direction. Moreover, several papers have been considering the relationship between vertical and lateral resistance (V-H space), Cathie et al. (2005), White and Randolph (2007), but the generalization into three dimensions seems to be missing.
In this paper we will present a simple and robust 3D model based on elasto-plasticity that is able to capture what the authors assess to be the most significant effects related to deepwater pipelines. Therefore issues like wave and current induced liquefaction are not considered. However, looking at the lateral response of pipelines under liquefaction, Foray et al. (2006), the overall behavior appear to follow the same patterns, hence the present model may with a few corrections be used for such applications as well.

PIPE-SOIL INTERACTION CHARACTERISTICS
Once in contact, the interaction between the pipeline and the soil can be described in terms of 3 degrees-of-freedom; penetration into the seabed (normal to the seabed), axial movements along the axis of the pipeline and lateral movement perpendicular to the pipeline. For each degree-of-freedom a model needs to capture certain characteristics.

Lateral resistance of partially embedded pipelines
The main purpose for developing the present model for pipe-soil interaction is to be able to account for the lateral resistance of unburied or partially embedded pipelines in case there is risk of e.g. lateral buckling. As emphasized e.g. by the SAFEBUCK project, Bruton et al. (2006), the lateral resistance is highly dependent on the magnitude of the lateral movement as well as by the load history. Considering Fig. 1 the resistance can be divided into various phenomena:

(1) At monotonic loading the lateral resistance curve exhibits at first a rather stiff, almost linear elastic response until it reaches the peak resistance. As the lateral movement increases further, the resistance level will gradually decrease to a residual resistance level. This might cause instability leading to e.g. lateral buckling of a pipeline.
(2) If the pipeline is unloaded the response is almost linear elastic until the lateral resistance is reached in the opposite direction.
(3) During cyclic loading it is observed that the overall behavior resembles that of the monotonic condition. There exists a peak, which is traditionally attributed to suction. Once this suction is released the lateral resistance reduces to a residual resistance.

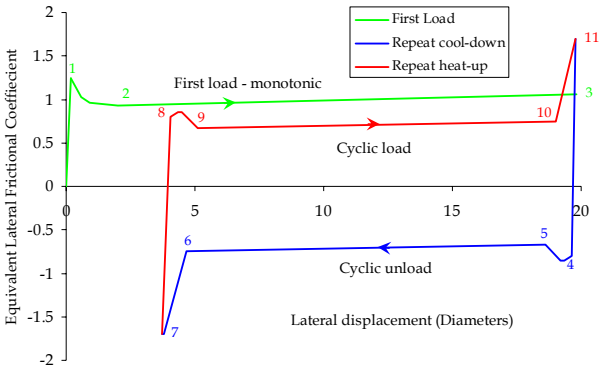

Figure 1. Principal lateral lateral behavior, Bruton et al. (2006)

(4) During sliding, it is also experimentally observed that there is a slight increase in resistance, which is assumed to be due to the gradual built up of an active berm in front of the pipeline.
(5) At reversed loading this berm remains in the extreme position, hence will act as a so-called dormant berm which may be reactivated in case the loading direction changes again. While the dormant berm certainly gives a significant resistance reserve, it is apparently only activated at very large movements, say 10D, hence it may not be important for practical design.

All these characteristics can be captured by an elasto-plastic model that is able to include a combination of isotropic and kinematic softening and hardening effects. The present model accounts for the first four items listed above, but can be expanded to include reactions from the dormant berm if required.

Axial resistance

The axial response is mainly activated during service condition of the pipeline. The behavior is influenced by the embedment and the loadThe axial response is mainly activated during service condition of the pipeline. The behavior is influenced by the embedment and the load-history. While the lateral response shows a slight increase due to the development of the active berm, the axial response of a pipeline does not show this effect. Therefore, the principal resistance curve does not display any hardening effects, see e.g. Dendani and Jaeck (2007). This is important to realize since it implies that a load-induced anisotropy will develop even if the combined axial and lateral resistance is initially isotropic. Hence, to realistically model the response of the pipe-soil interaction, we must make sure that the model is able to account for this anisotropy.

Penetration resistance

The (vertical) penetration of the pipeline into the seabed is an important parameter in the development of axial and lateral resistance - either in terms of pure frictional resistance or through a combination of lateral earth pressure, adhesion and friction. The description of the vertical penetration-resistance relation is thus a basic part of any model for sliding resistance. However, in the context of the present model, it is not critical which model is chosen. Several exist, such as those prescribed in offshore pipeline codes from DNV or BS, or relations developed by various researchers like e.g. Verley and Lund (1995) and Verley and Sotberg (1994).

ELASTO-PLASTIC MODEL

Traditionally, the theory of plasticity is formulated in terms of strains and conjugate stresses. For contact problems, which often involves discontinuities, the use of strain formulation is inconvenient. Instead the model is formulated in terms of displacements and conjugate forces. Still, the basic assumption for rate independent plasticity is used so that the total displacement increment is decomposed into an elastic, $d\mathbf{u}^e$, and a plastic part, $d\mathbf{u}^p$, i.e.

$$d\mathbf{u} = d\mathbf{u}^e + d\mathbf{u}^p \tag{1}$$

where $d\mathbf{u}^T = (du_x\, du_y\, du_z)$ with the first two components representing the two sliding[1] components and the third term being the vertical (normal) component. Conjugate to the displacements are the sliding forces q_x, q_y and the normal force q_z (positive in tension in order to comply with standard finite element conventions) acting on the sliding plane.
The force increment is defined using the elastic stiffness, $\mathbf{C}$,

$$d\mathbf{q} = \mathbf{C}\; d\mathbf{u}^e = \mathbf{C}\,(d\mathbf{u} - d\mathbf{u}^p) = \mathbf{C}\left(d\mathbf{u} - d\lambda \frac{\partial g}{\partial \mathbf{q}^T}\right) \tag{2}$$

where the plastic strain increment is determined using the flow rule $d\lambda\, \partial g/\partial \mathbf{q}^T$ is introduced. The stress increment is subject to the constraint that the yield condition is fulfilled

$$f(\mathbf{q}, \boldsymbol{\kappa}) \leq 0 \tag{3}$$

Here the state parameters, $\boldsymbol{\kappa}$, are introduced.
The formulation of the specific model is done with reference to this elasto-plastic framework.

Yield condition

The present model is based on a simple Coulomb friction model with cohesion as defined by Krenk (2004). The formulation is further expanded to account for hardening and degradation effects. It is deliberately chosen to retain the friction format in order to facilitate the numerical implementation. Using the friction format, the model furthermore by default embeds a kinematic hardening model, which – considering the cyclic nature of the governing loads – is very convenient.
The model is expressed in terms of forces $\mathbf{q}^T = (q_x\, q_y\, q_z)$. For a constant normal force the sliding condition is given as

$$\left(\frac{q_x}{q_x^0}\right)^2 + \left(\frac{q_y}{q_y^0}\right)^2 = 1 \tag{4}$$

where q_x^0 and q_y^0 are the sliding strength corresponding to the current normal force q_z. The current sliding strength thus is depending on the normal force acting on the sliding plane. Including a cohesive strength, the classical Coulomb friction model may be written as

$$\begin{aligned} q_x^0 &= \mu_x p(c, q_z) \\ q_y^0 &= \mu_y p(c, q_z) \end{aligned} \tag{5}$$

The friction coefficients in the two directions are denoted μ_x and μ_y, respectively. The nominal normal force $p(c, q_z)$ is function of the current normal force (positive in tension) acting on the

[1]The notion *sliding* refers to the combined axial and lateral movement of the pipeline.

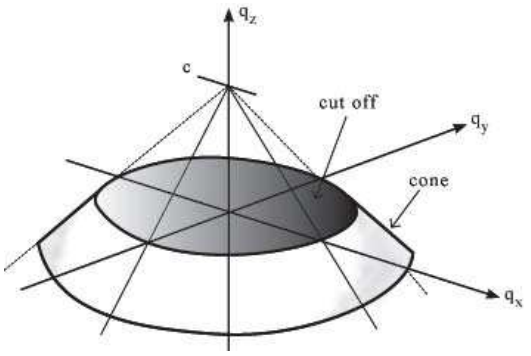

Figure 2. Truncated friction yield surface

sliding plane q_z and a constant (cohesive) term c. The classical Coulomb model is represented as a linear function, i.e.

$$p(c, q_z) = c - q_z \tag{6}$$

Alternatively, it is possible to take into account the coupling between sliding resistance and penetration resistance (V-H-space) using a non-linear function e.g. of the format

$$p(c, q_z) = \left(1 - \left(\frac{|q_z|}{q_{z,ult}}\right)^{\alpha}\right)(c - q_z) \tag{7}$$

The limiting strength $q_{z,ult}$ is the ultimate penetration capacity. In this way the sliding capacity is reduced depending on the degree of mobilization of the penetration capacity with vanishing sliding resistance at fully mobilized penetration resistance.
Introducing Eq. (5) into Eq. (4) and rearranging the equation yields

$$\left(\frac{q_x}{\mu_x}\right)^2 + \left(\frac{q_y}{\mu_y}\right)^2 = p^2 \tag{8}$$

For the use in an elasto-plastic model, Eq. (8) can be reformulated to a linear format, i.e.

$$f(\mathbf{q}) = \sqrt{\left(\frac{q_x}{\mu_x}\right)^2 + \left(\frac{q_y}{\mu_y}\right)^2} - p = 0 \tag{9}$$

In addition to the sliding strength, a limit to the normal force may be imposed, i.e.

$$q_z - q_z^0 = 0 \tag{10}$$

in which q_x^0 is the bearing capacity as function of the penetration. The resulting yield function for the linear Coulomb model thus becomes a truncated cone in the stress space, see Fig. 2. The cut-off at the bottom of the cone is governed by the vertical bearing capacity, hence will limit the maximum sliding resistance.
The gradient to the yield function with respect to $\mathbf{q}$ is thereby

$$\frac{\partial f}{\partial \mathbf{q}} = \left[\frac{q_x/\mu_x^2}{p} \quad \frac{q_y/\mu_y^2}{p} \quad -\frac{dp}{dq_z}\right] \tag{11}$$

It is thus seen that the gradient is always acting in the direction of the total force vector in the sliding plane.

Flow rule
In case of plastic loading, the plastic displacement increment is given as

$$d\mathbf{u}^p = d\lambda \frac{\partial g}{\partial \mathbf{q}^T} \tag{12}$$

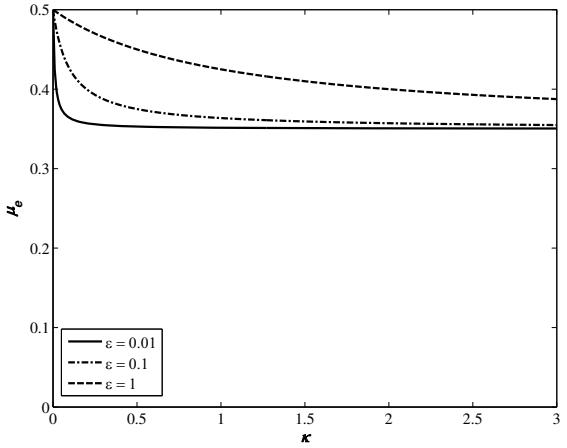

Figure 3. Degradation of friction coefficient, $\mu_{peak} = 0.5$, $\theta = 0.3$

The flow rule for the sliding problem is assumed to be associated in the sliding plane. At least for isotropic friction there seems to be no physical evidence to suggest otherwise. However, the normal (vertical) component may either be associated or non-associated. A general format of the flow rule is thus

$$\frac{\partial g}{\partial \mathbf{q}} = \left[\frac{q_x/\mu_x^2}{p} \quad \frac{q_y/\mu_y^2}{p} \quad \gamma\right] \tag{13}$$

where $\gamma = 1$ corresponds to associated flow, i.e. plastic sliding will produce upward movement of the sliding plane. For a non-dilatant sliding model $\gamma = 0$. The choice of flow rule for the normal component heavily influences the implementation strategy for the numerical algorithm. Here, the simplest possible version of a friction model will be used in combination with a vertical elasto-plastic bearing capacity model. Using a non-dilatant flow rule for the sliding problem decouples the vertical strength from the horizontal strength. Therefore the two parts may be solved sequentially, first establishing the normal force and then solving the sliding problem. This simplifies immensely the development of efficient integration algorithms for the model and also allows implementation of complex hardening/degradation mechanism for the sliding resistance.

Degradation model for sliding resistance
Often it is observed that the sliding resistance of a pipeline that is not embedded shows degradation from a peak resistance q_{peak} to a residual resistance q_{res} due to either large movements or cyclic loading. This effect may conveniently be described in terms of a degradation model such that the friction capacity reduces from its peak value to its residual value depending on the governing state parameter, κ.

$$q_\alpha^0(\kappa) = q_{peak} - d(\kappa)\,(q_{peak} - q_{res}) \quad ; \quad \alpha = x, y \tag{14}$$

with the degradation function $d(\kappa)$ increasing monotonically from 0 to 1 as the state parameter κ evolves. Defining the ratio $\theta = (q_{peak} - q_{res})/q_{peak}$ enables us to rewrite Eq. (14) as

$$q_\alpha^0(\kappa) = p(c, q_z)\,\mu_e(\kappa) \tag{15}$$

thus defining the effective friction as

$$\mu_e(\kappa) = \mu_{peak}(1 - \theta\, d(\kappa)) \tag{16}$$

The degradation function can be chosen arbitrarily. Here the following format is chosen in order to allow for easily inversion of the function,

$$d(\kappa) = \frac{\kappa}{\kappa + \varepsilon} \tag{17}$$

The parameter ε controls the rate of degradation as illustrated in Fig. 3 and may be calibrated to actual measurements.

ANISOTROPIC SLIDING RESISTANCE MODEL

The basic sliding model presented above may be generalized by introduction of a matrix formulation. This is done in order facilitate the introduction of hardening or degradation.

Introducing the sliding force vector $\mathbf{q}_s^T = (q_x\, q_y)$ enables us to define the sliding yield function for a given normal force q_z a

$$f_s = \sqrt{\mathbf{q}_s^T \mathbf{M}^T \mathbf{M} \mathbf{q}_s} - p\,(c, q_z) \leq 0 \tag{18}$$

The matrix $\mathbf{M}$ contains the friction coefficients,

$$\mathbf{M}(\boldsymbol{\kappa}) = \begin{bmatrix} \dfrac{1}{\mu_x(\boldsymbol{\kappa})} & 0 \\ 0 & \dfrac{1}{\mu_y(\boldsymbol{\kappa})} \end{bmatrix} \tag{19}$$

The present format is identical to the formulation presented by e.g. Feng et al. (2006) - except for the dependency of the friction coefficients on the state parameters. The dependency on the state parameters is introduced via a multiplicative format

$$\mathbf{M}(\boldsymbol{\kappa}) = \mathbf{M}_0 \mathbf{H}_i(\kappa_1) \mathbf{H}_k(\kappa_2, \kappa_3) \tag{20}$$

in which

$$\mathbf{M}_0 = \begin{bmatrix} \dfrac{1}{\mu_x^0} & 0 \\ 0 & \dfrac{1}{\mu_y^0} \end{bmatrix} \tag{21}$$

is the peak friction at monotonic loading. The modifying terms $\mathbf{H}_i$ and $\mathbf{H}_k$ represent the isotropic hardening/degradation and the kinematic hardening/degradation, respectively.

Based on the principal behavior described in Fig. 1 the isotropic degradation term in Eq. (20) is introduced in order to account for the reduction from peak to residual strength for monotonic sliding. The isotropic degradation term is using the total accumulated equivalent plastic displacements κ_1 as state parameter.

$$\mathbf{H}_i(\kappa_1) = \begin{bmatrix} \dfrac{1}{h_i(\kappa_1)} & 0 \\ 0 & \dfrac{1}{h_i(\kappa_1)} \end{bmatrix} \tag{22}$$

with

$$h_i(\kappa) = \left(1 - \theta_i \frac{\kappa}{\kappa + \varepsilon_i}\right) \tag{23}$$

Notice that the degradation term leads to a general reduction of the friction capacity as illustrated on Fig. 3. The associated state parameter is chosen as the accumulated plastic displacements, i.e.

$$d\kappa_1 = \sqrt{(d\mathbf{u}^p)^T d\mathbf{u}^p} = d\lambda \sqrt{\left(\frac{\partial g}{\partial \mathbf{q}^T}\right)^T \frac{\partial g}{\partial \mathbf{q}^T}} \tag{24}$$

The second term in Eq. (20) is a kinematic term representing both a large displacement degradation and a linear kinematic hardening term to model the build up of an active berm. The kinematic state parameters are κ_2 and κ_3 that are the plastic displacement in lateral and axial directions, respectively, accumulated within a single load cycle. Hence κ_2 is reset in case the direction of the lateral movement is reversed and κ_3 is reset if the axial movement is reversed.

$$\mathbf{H}_k(\kappa_2, \kappa_3) = \begin{bmatrix} \dfrac{1}{h_k^x(\kappa_2)} & 0 \\ 0 & \dfrac{1}{h_k^y(\kappa_3)} \end{bmatrix} \tag{25}$$

with

$$h_k(\kappa) = (1 + H\kappa)\left(1 - \theta_k \frac{\kappa}{\kappa + \varepsilon_k}\right) \tag{26}$$

In principle all parameters for the kinematic hardening function h_k^x and h_k^y may be selected independently in the two directions. However, the motivation for introducing the linear hardening term is based on the development of the active berm during lateral movement whereas the degradation term accounts for suction release and cyclic degradation which is common to both directions. Hence here we only allow for the hardening moduli to be different in lateral and axial direction, i.e. $H_x \neq H_y$. The state parameters are the plastic deformation accumulated during the current load cycle, i.e.

$$d\kappa_2 = |du_1^p| = d\lambda \left|\frac{\partial g}{\partial q_1}\right| \tag{27}$$

and

$$d\kappa_3 = |du_2^p| = d\lambda \left|\frac{\partial g}{\partial q_2}\right| \tag{28}$$

The effect of the kinematic term is that the sliding resistance first reduces and then starts to increase due to the linear hardening term.

It is worth noticing that the multiplicative format allows for easy addition of other effects, e.g. the dependency of the hardening modulus on penetration depth. Furthermore, we can introduce a coupled friction model simply by letting the off-diagonals be different from zero.

Elasticity

The elastic part of the sliding model is for demonstration purposes chosen as the simplest possible, i.e. uncoupled and linear. Hence the elastic stiffness $\mathbf{C}_s$ is written as

$$\mathbf{C}_s = \begin{bmatrix} E_x & 0 \\ 0 & E_y \end{bmatrix} \tag{29}$$

In reality the stiffness in frictional contact is in general non-linear with respect to the contact pressure as well as the magnitude of sliding. The coupling terms - omitted in the present version - accounting for the Poisson effects should also be included in a more refined elasticity model.

PENETRATION MODEL WITH EMBEDDED CONTACT

The representation of the penetration resistance is also modeled using the elasto-plastic framework. The penetration resistance curve is discretized into a piecewise linear format thus allowing for arbitrary relations to be implemented. Here the relation for soft clay by Verley and Lund (1995) is used. The model is formulated in terms of an isotropic hardening plasticity model, i.e.

$$f_p(q_z, \kappa_z) = q_z - q_z^0(\kappa_z) \leq 0 \tag{30}$$

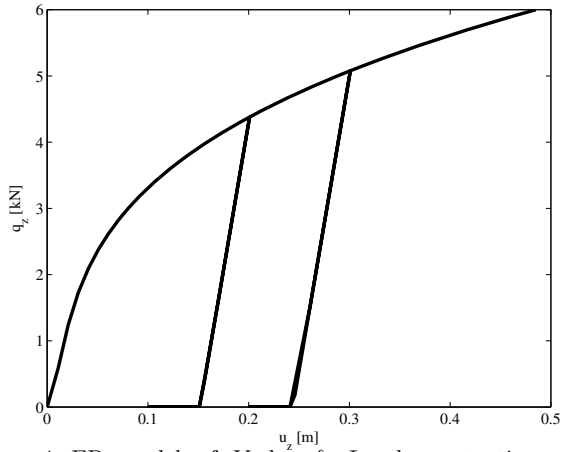

Figure 4. EP model of Verley & Lund penetration model

with the state parameter

$$\kappa_z = \int du_z^p \tag{31}$$

being the accumulated plastic displacement of the soil.
One of the challenges of using the format by Verley and Lund (1995) is to define a representative elastic stiffness E_z, since the model - due to the S-shape of the relation at low penetration depths - does not prescribe a monotonically decreasing stiffness. In the present application E_z is chosen to be 1.5 times the maximum secant modulus in order to ensure uniqueness of the constitutive relation.

Embedded contact algorithm
A special issue for pipeline analysis is the possibility for the pipeline to unload and loose contact. This feature may of course be handled by a contact algorithm, but may also be embedded into the penetration model. Considering the unloading/reloading phase as non-linear elastic region, the loss of contact may be accounted for by introducing a very small stiffness – "zero" stiffness – once the total penetration[2] $-u_z$ becomes less than the plastic displacement of the soil, κ_z. Taciroglu et al. (2006) proposed a format that gives a continuous transition from "zero" stiffness to finite stiffness,

$$E_z(u_z, \kappa_z) = E_z^0 \frac{1}{2^{(u_z+\kappa_z)/\rho} + 1} \tag{32}$$

in which ρ controls the steepness of the transition. The penetration model with embedded contact is demonstrated in Fig. 4. As it is seen, the model is capable of representing the classical effects of pre-consolidation. This will especially be of importance during pipelay analysis where there tends to be significant over-penetration at the touch-down point.

EXAMPLES
Model tests have been carried out to demonstrate the ability of the model to capture the observed behavior of pipe-soil interaction. The examples have been defined in such a way, that they also test the robustness of the model and its numerical implementation. The general material properties used in all examples are listed in Table 1 and the properties of the sliding model are listed in Table 2. All tests have been carried out using prescribed displacement patterns. All tests have first been preloaded vertically following the penetration curves representing soft clay. Next, sliding tests have been carried out - either in lateral direction u_x or in a combination of lateral movement, u_x, and axial movement, u_y.

Table 1. Pipe and soil properties

Pipe diameter	D	0.27 m
Unit weight	γ_s	16 kN/m^3
Undrained shear strength	s_u	4 kPa
Elastic modulus (penetration)	E_z	89 kN/m
Elastic modulus (sliding)	$E_x = E_y$	10 kN/m

Table 2. Properties for sliding model

No	μ_x^0	μ_y^0	ε_i	θ_i	ε_k	θ_k	H_x	H_y
Example 1	0.5	0.5	0.3	0.1	0	0	0	0
Example 2	0.5	0.5	0.3	0.1	0	0	0	0
Example 3	0.5	0.3	0.3	0.1	0	0	0	0
Example 4	0.5	0.5	0.3	0.2	0.5	0.2	0.7	0
Example 5	0.5	0.5	0.3	0.2	0.5	0.2	0.7	0
Example 6	0.5	0.5	0	0	0	0	0	0

Example 1: Monotonic lateral sliding
The first example is defined in order to assess that the degradation model works correctly. The displacement resistance curve is shown in Fig. 5. It is seen that the peak resistance corresponds exactly to $\mu_x q_z$, furthermore it is seen that the residual resistance is 30% smaller than peak resistance ($\theta_i = 0.3$).
The efficiency of the numerical integration algorithm is essential to the implementation of the model into a pipeline analysis program. As seen from Fig. 5 it is possible to trace the resistance curve for a lateral movement of almost 2D rather accurately with only 30 load increments. The convergence of each increment was in both cases obtained for 5-7 iterations. Hence, the computational cost does not increase significantly with larger increments. More importantly, the algorithm remains robust even for larger

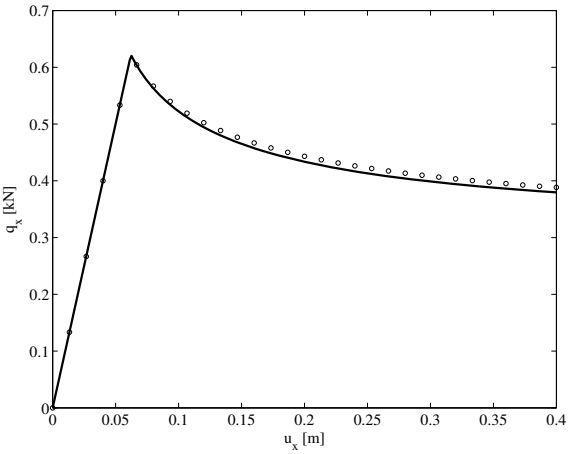

Figure 5. Monotonic lateral sliding, $q_z = 1.24$kN, (− exact, ∘ 30 steps)

[2]Penetration is negative due to sign convention

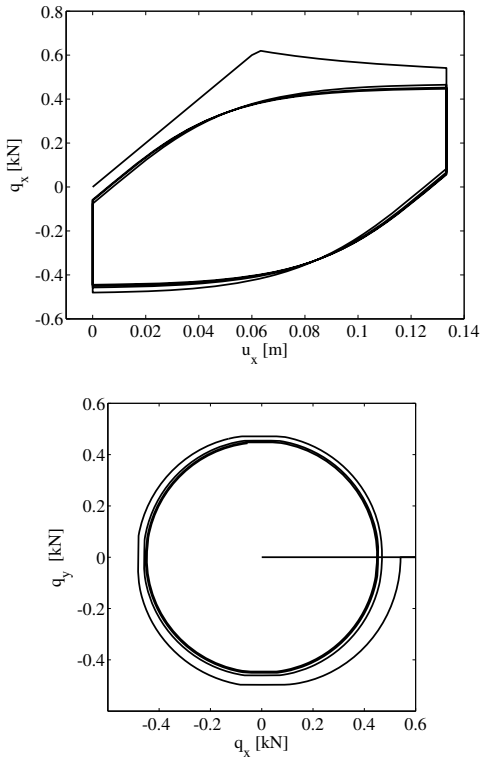

Figure 6. Circular sliding of isotropic model, $q_z = 1.24$kN

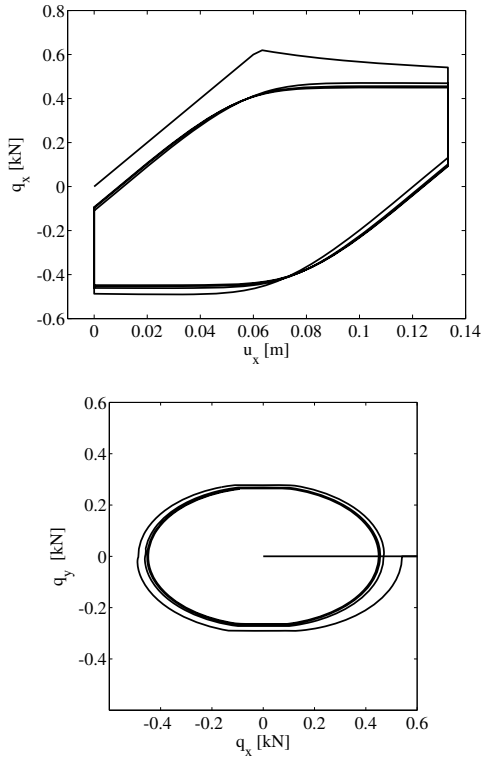

Figure 7. Circular sliding of anisotropic model, $q_z = 1.24$kN

load increments.

Example 2: Isotropic sliding model with degradation
The second example illustrates how the degradation gradually reduces the sliding capacity. The model is loaded in cycles of 4 sub-steps by a displacement pattern describing a square, i.e.

$$\begin{array}{ll} \text{Sub-step 1:} & \Delta u_x > 0 \quad \Delta u_y = 0 \\ \text{Sub-step 2:} & \Delta u_x = 0 \quad \Delta u_y < 0 \\ \text{Sub-step 3:} & \Delta u_x < 0 \quad \Delta u_y = 0 \\ \text{Sub-step 4:} & \Delta u_x = 0 \quad \Delta u_y > 0 \end{array}$$

The response is shown in Fig. 6. It is seen that the model traces the degrading yield function as it is suppose to, thus forming a spiral. The horizontal line in the (q_x, q_y) diagram represents the elastic loading which is exhausted already in the first sub-step.

Example 3: Anisotropic sliding model with degradation
To see the effect of anisotropy, the same load pattern as in example 2 is applied to a model with anisotropic friction $\mu_x = 0.5$ and $\mu_x = 0.3$. Again the model traces the yield function, cf. Fig. 7. It is however no longer circular, but elliptic as expected.

Example 4: Cyclic lateral sliding with kinematic degradation and hardening
The full potential of the model is utilized in case of cyclic loading taking account of both the overall degradation effect in terms of the isotropic term and the cyclic effects represented by the kinematic degradation/hardening model. The load pattern is a number of lateral cycles $\Delta u_x = \pm\Delta u$, $\Delta u_y = 0$. The results in Fig. 8 first follows the monotonic degradation curve, but as the displacement increases the hardening term starts to dominate. This leads to an increase in resistance capacity. At unloading the response is at first elastic until the lateral resistance is reached. Notice that as the model cycles it ends up at a state for which the resistance curves become a closed loop – a feature that is actually observed from model tests, Bruton et al. (2005) The number of cycles necessary to reach this state can be controlled by selecting the isotropic degradation scale ε_i appropriately.

Example 5: Cyclic sliding with kinematic degradation and hardening with combined loading
The previous example considered only sliding in lateral direction.

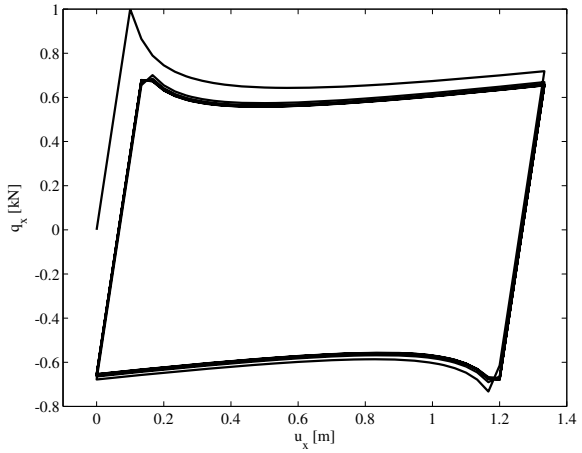

Figure 8. Cyclic sliding with kinematic degradation and hardening, $q_z = 2.09$kN

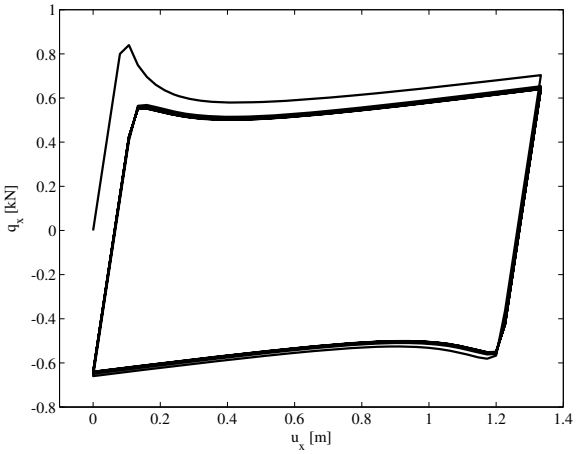

Figure 9. Cyclic sliding with kinematic degradation and hardening, $\Delta u_y/\Delta u_x = 0.5$, $q_z = 2.09$kN

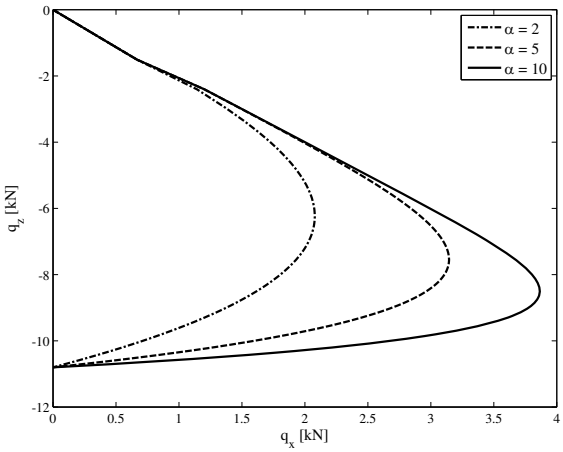

Figure 10. Combined penetration and sliding - coupled response

In case of lateral buckling, part of the pipeline will also move axially. In order to see the effect of such a movement, displacement cycles with a constant ratio between $\Delta u_y/\Delta u_x = 0.5$ have been analyzed. It is seen, Fig. 9 that the lateral capacity is influenced by the axial component. In the present case the axial component the lateral resistance is reduced by approximately 10%.

Example 6: Combined penetration and lateral movement

The possibility to reduce the sliding capacity at increasing mobilization of the penetration resistance only has limited relevance for partially embedded pipelines. Still, in Fig. 10 the coupled response, cf. Eq. (7), is demonstrated for different values of the exponent α. It is seen that for increasing values of α, the response approaches the linear Coulomb friction model, Eq. (6).

CONCLUSIONS

A robust and versatile spring element for pipe-soil interaction analysis has been presented. The model is formulated in a three dimensional elasto-plastic framework allowing for coupling of penetration and combined axial and lateral movement. A robust numerical implementation is developed in order to facilitate the integration of the spring element into a finite element code for pipeline analysis. The capability of the model is tested by several examples demonstrating that the model is able to capture essential features of partially embedded pipelines, such as transition from peak to residual resistance under monotonic loading and cyclic performance accounting for both suction release and active berm development. The elasto-plastic framework with a multiplicative hardening/degradation formulation allows for easy extension of the model. Furthermore, embedment of a contact algorithm into the penetration part and a possible coupling between mobilized sliding and penetration resistance adds to the capabilities of the model without any significant computational costs.

The calibration of the model parameters has not been considered in this article. However, the degradation parameters are relatively easily obtained from the lateral resistance measurements e.g. presented by Bruton et al. (2007). Furthermore, the penetration properties are directly obtained from the chosen penetration model. Hence the outstanding model parameters are the elastic moduli for axial and lateral movements and the kinematic hardening modulus. These parameters are most likely highly dependent on the normal pressure. Therefore, in order to achieve more realistic values it is probably necessary to include a dependency on the penetration depth. This dependency is however, not difficult to include in the present formulation.

It is the author's opinion that application of the the current model in practical pipeline design will enable a realistic prediction of the behavior, especially for large displacement and cyclic loading, since it is able to capture the observed degradation mechanisms and development of an active berm in lateral direction. The model accounts for the load-history of the soil, which significantly affects the soil capacity - both related to penetration and sliding. Additionally, the EP model is a true 3D model instead of 3 x 1D decoupled spring elements, which ensures that the model can describe the full stress plane at any given penetration, and thus is less dependent of specific spring curves entered by the designer. The designer is hereby offered a tool for carrying out parametric studies and investigate multiple scenarios, which in turn is a prerequisite for a better and more reliable pipeline design.

REFERENCES

Bruton, D., M. Carr, M. Crawford, and E. Poiate (2005). The safe design of hot on-bottom pipelines with lateral buckling using the design guideline developed by the safebuck joint industry project. In *Proc. Deep Offshore Technology Conference, Brazil 2005*.

Bruton, D., M. Carr, and D. White (2007). The influence of pipe-soil interaction on lateral buckling and walking of pipelines - the safebuck jip. In *Proc. 6th International Offshore Site Investigation and Geotechnics Conference*, pp. 133–148.

Bruton, D., D. White, C. Cheuk, M. Bolton, and C. M. (2006). Pipe/soil interaction behavior during lateral buckling, including large-amplitude cyclic displacement tests by safebuck jip. In *Proc. Offshore Technology Conference*, Number Paper No. OTC 17944.

Cathie, D., C. Jaeck, J.-C. Ballard, and J.-F. Wintgens (2005). Pipeline geotechnics - state-of-the-art. In Gourvenec and

Cassidy (Eds.), *Frontiers in Offshore Geotechnics: ISFOG 2005*. Taylor & Francis Group.

Cheuk, C., D. White, and M. Bolton (2007). Large-scale modelling of soil-pipe interaction during large amplitude cyclic movements of partially embedded pipelines. *Canadian Geotechnical Journal 44*, 977–996.

Dendani, H. and C. Jaeck (2007, September). Pipe-soil interaction in highly plastic clays. In *Proc. 6th International Offshore Site Investigation and Geotechnics Conference*, pp. 115–124.

Feng, Z., M. Hitaj, de Saxcé G., and Z. Mróz (2006). Effect of frictional anisotropy on the quasistatic motion of a deformable solid sliding on a planar surface. *Journal of Computational Mechanics 37*, 349–361.

Foray, P., D. Bonjean, H. Michallet, and M. Mory (2006). Fluid-soil-structure interaction in liquefaction around a cyclically moving cylinder. *Journal of Waterway, Port, Coastal and Ocean Engineering, ASCE 132*(4), 289–299.

Krenk, S. (1993). *Non-linear analysis with finite element*. Aalborg University.

Krenk, S. (2004). A pipeline friction model. Technical University of Denmark (unpublished note).

Lambrakos, K. (1985). Marine pipeline soil friction coefficients from *in-situ* testing. *Journal of Ocean Engineering 12*(2), 131–150.

Simo, J. and M. Ortiz (1985). A unified approach to finite deformation elastoplastic analysis based on the use of hyperelastic constitutive equations. *Computer methods in applied mechanics and engineering 49*, 221–245.

Taciroglu, E., C. Rha, and J. Wallace (2006, October). A robust macroelement model for soil-pile interaction under cyclic loads. *Journal of Geotechnical and Geoenvironmental Engineering, ASCE 132*(10), 1304–1314.

Verley, R. and K. Lund (1995). A soil resistance model for pipelines placed on clay soils. In *Proc. of OMAE 1995*, Volume Volume V, Pipeline Technology, pp. 225–232.

Verley, R. and T. Sotberg (1994). A soil resistance model for pipelines placed on sandy soils. *Journal of Offshore Mechanics and Arctic Engineering 116*, 145–153.

White, D. J. and M. Randolph (2007). Seabed characterisation and models for pipeline-soil interaction. *International Journal of Offshore and Polar Engineering 17*, 193–204.